ACS **Medicinal** Chemistry *Letters*

Optimization of Nicotinamides as Potent and Selective IRAK4 Inhibitors with Efficacy in a Murine Model of Psoriasis

Satheesh Nair,* Sreekantha Ratna Kumar, Venkatram Reddy Paidi, Ramesh Sistla, Durgarao Kantheti, Subba Rao Polimera, Soodamani Thangavel, Amrita Jha Mukherjee, Mitalee Das, Rajeev S. Bhide, William J. Pitts, Natesan Murugesan, Shailesh Dudhgoankar, Jignesh Nagar, Siva Subramani, Debarati Mazumder, Julie A. Carman, Deborah A. Holloway, Xin Li, Mark P. Fereshteh, Stefan Ruepp, Kamalavenkatesh Palanisamy, T. Thanga Mariappan, Srinivas Maddi, Ajay Saxena, Paul Elzinga, Anjaneya Chimalakonda, Qian Ruan, Kaushik Ghosh, Sucharita Bose, John Sack, Chunhong Yan, Susan E. Kiefer, Dianlin Xie, John A. Newitt, S. Pon Saravanakumar, Richard A. Rampulla, Joel C. Barrish, Percy H. Carter, and John Hynes, Jr.*

Read Online

ACCESS | Metrics & More | Article Recommendations | Supporting Information

ABSTRACT: IRAK4 is an attractive therapeutic target for the treatment of inflammatory conditions. Structure guided optimization of a nicotinamide series of inhibitors has been expanded to explore the IRAK4 front pocket. This has resulted in the identification of compounds such as **12** with improved potency and selectivity. Additionally **12** demonstrated activity in a pharmacokinetics/pharmacodynamics (PK/PD) model. Further optimization efforts led to the identification of the highly kinome selective **21**, which demonstrated a robust PD effect and efficacy in a TLR7 driven model of murine psoriasis.

KEYWORDS: IRAK4, kinase, lupus, TLR, psoriasis

20, X = H
IRAK4 IC$_{50}$ 3.2 nM, SI 7.8
21, X = F
IRAK4 IC$_{50}$ 3.4 nM, SI 1.0
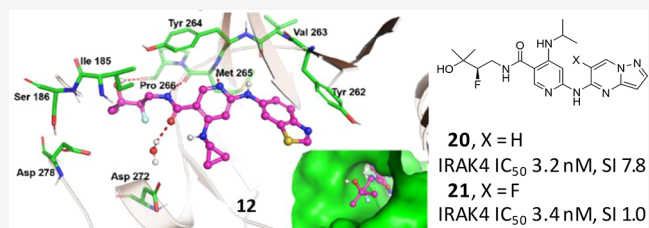
Interleukin-1 receptor associated kinase 4 (IRAK4) activity is integral to the signaling of Toll-like receptors (TLR) and interleukin-1 family receptors (IL-1R).[1] A wide variety of stimuli including cellular or bacterial degradation products activate TLRs. These activated receptors in turn lead to the recruitment of intracellular adapter proteins, such as MyD88, and kinases including IRAK4 and IRAK1.[2,3] The resulting complex, referred to as the myddosome, activates TRAF6 and TAK1, leading to the production of pro-inflammatory signaling molecules, such as tumor necrosis factor α (TNF-α) and interleukin-6 (IL-6).[4]

Animals lacking functional IRAK4 are resistant to TLR agonist induced cytokine production and have reduced responses in murine models of inflammatory disease.[5] In IRAK4 deficient mice, IL-1 receptor and TLR signaling is severely impaired.[6] Additional genetic validation has come from human patients lacking functional IRAK4, in which immune cells obtained from these patients have a diminished response to TLR agonists, IL-1β, and IL-18.[7,8] Overall, the combined human and mouse observations suggest that therapeutic blockade of this pathway may have beneficial effects in human disease. Recently, we reported a potent and selective IRAK4 inhibitor with efficacy in murine models of lupus suggesting promise for the treatment of systemic lupus erythematosus (SLE) in humans.[9] In addition to our efforts, a number of diverse small molecule inhibitors have been reported[10] with the most advanced compound, PF-06650833, in phase 2 clinical trials for rheumatoid arthritis.[11,12]
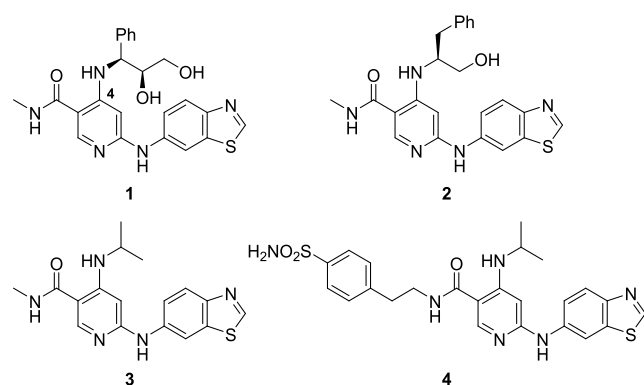
We have previously reported the discovery of a series of small molecule IRAK4 inhibitors and identified (**1**, Figure 1) as a lead compound with excellent IRAK4 enzyme activity and moderate kinome selectivity[13] (SI$_{33}$[14] of 9.7). However, **1** and the close analog **2** suffered from poor Caco-2 permeability preventing advancement to in vivo efficacy studies. We postulated that the alcohol functionality might be contributing to the poor Caco-2 permeability and through a series of straightforward modifications of the C4 substituent, identified **3**. In addition to maintaining IRAK4 potency, an increase in Caco-2 permeability was observed with this modification. At this point in our effort we chose to maintain the C4 substituent as in **3** and optimize subsequent analogs with respect to kinome selectivity and

Figure 1. Early lead compounds and key data. [a]Kinase and PBMC assays were run in triplicate unless otherwise noted. Values represent mean $IC_{50} \pm$ SD. [b]Caco-2 permeability, liver microsomal stability, and kinome selectivity assays were typically single determinations.

Assay	1	2	3	4
IRAK4 IC_{50} (nM)[a]	4.7 ± 3.6	11 (n=2)	21 (n=1)	5.7 (n=1)
PBMC IC_{50} (nM)[a] (LTA→IL6)	300 ± 360	$2,900 \pm 2,700$	4,500 (n=1)	1,200 (n=2)
Fold Sel Lck	16	37	28	280
Caco-2 A→B (nm/s)[b]	<15	< 15	210	<15
LM Stability (H / Ms % rem)	90 / 22	46 / 29	nt	17 / 38
Kinome SI33[b]	9.7	11	9.7	0.7

functional potency in IRAK4 mediated cellular and whole blood assays. In general the series was moderately selective across the kinome; however compounds exhibited low selectivity against some tyrosine kinase family members, such as Lck.[15] Since inhibition of Lck could confound interpretation of efficacy data (adaptive versus innate immunity), we counterscreened against Lck routinely as a coarse measure of analog selectivity.

The IRAK4 protein is amenable to cocrystallization, and the X-ray cocrystal structure of **2** with the IRAK4 kinase domain has been previously disclosed.[13] The IRAK4 kinase domain has a bilobal structure typical of kinases. In addition, two insertion loops give a distinct character to the region adjacent to the extended hinge region (known as the front pocket) of IRAK4. The first insertion loop in the N-terminus is a Schellman type loop, which contains hydrophobic amino acids such as Pro184, Ile185, and Val187, as well as the hydrophilic amino acid Ser186. A second insertion loop in IRAK4 is known as the α-D loop.[16] The presence of these two loops in the usually solvent filled front pocket of other kinases provides a tunnel like shape to this region with both hydrophobic and polar residues lining the surface. We reasoned that effective engagement of this "front pocket" could improve kinome selectivity. The tyrosine gatekeeper residue is another unusual feature of IRAK4 (Tyr262). We also postulated that an optimized π-stacking interaction with Tyr262 could be effectively differentiated from kinases, which have a phenylalanine as a gatekeeper residue.

Utilizing this information, we focused our initial efforts on extending the amide side chain to engage interactions from N-terminal residues, such as Ile185 and Ser186, in the Schellman loop. A diverse amide library was prepared, which led to the identification of **4**. We were gratified to find that the phenethyl substituted **4** displayed a moderate improvement in biochemical potency and a noted improvement in kinome selectivity relative to compounds **1**–**3**. The structure of **4** was modeled into IRAK4

(Figure 2) and highlights a potential interaction of the sulfonamide with Asp278 and possibly Ile185. These additional
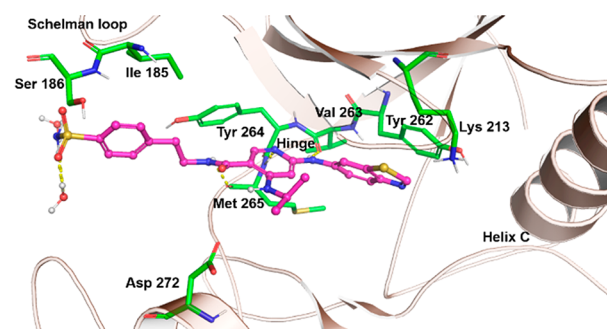

Figure 2. Compound **4** modeled into IRAK4, which depicts potential additional interactions with the front pocket. Residues involved in hydrogen bonds are labeled, and H-bonds are shown by dotted lines. Atom color code: yellow, sulfur; red, oxygen; blue, nitrogen; green, protein carbons; magenta, ligand carbons.

interactions relative to **3** could explain the improved kinome selectivity. However, in vitro profiling data for **4** revealed several issues including poor liver microsomal stability across species (<40% remaining after 10 min, mouse), significant CYP3A4 inhibition (IC_{50} 0.9 nM), and reduced Caco-2 permeability compared to **3**. Despite this unfavorable profile, we were encouraged by the observed enhancements with compound **4** that could be gained by engaging the front pocket.

We proceeded to conduct a more systematic amide SAR study (Table 1) to identify preferred substitution patterns. An increase in the length of simple alkyl chains (**5**–**7**) had no effect on IRAK4 enzyme potency. Molecular modeling suggested that a propanol fragment could engage in a H-bond with the extended hinge region of the kinase (Pro266) leading to the synthesis of **8**. The addition of the terminal gem-dimethyl group in analogs **9**–**12** and **14** and **15** generally led to an increase in biochemical potency. More importantly, notable increases in both cellular (IC_{50} 230–730 nM) and human whole blood potency (IC_{50} 810–2800 nM) relative to **8** were observed. Additionally, these compounds were >100-fold selective over Lck and had improved liver microsomal stability relative to the non-hydroxylated analogs (**5**–**7**). Fluorine was introduced at the beta position of the gem-dimethyl alcohol substituent (**11**, **12**) in an effort to improve liver microsomal stability compared to the desfluoro analogs **9** and **10**.[17] This substitution provided moderate gains in human liver microsomal stability (see **10** to **12**, 65% to 90% remaining). Mouse liver microsomal stability was marginally affected with this change. Replacement of the fluoro group with a methyl group (**13**) resulted in the loss of enzyme and cellular potency. The gem-difluoro analog **14** provided moderate functional potency in PBMCs with an associated reduction in whole blood potency. The enantiomer of **12**, compound **15**, trended less potent than **12** and was not studied further. Kinome-wide selectivity for **11** (SI_{33} 2.5) and **12** (SI_{33} 1.7) was improved over compounds **1**–**3** (SI_{33} ~10). In summary, this amide SAR study resulted in the identification of compounds with improved potency, selectivity, and metabolic stability over earlier analogs (**1**–**3**, **7**), and compound **12** appeared to be a suitable candidate for further study.

The X-ray cocrystal structure of **12** bound to IRAK4 (Figure 3) showed that the amide side chain at C5 projects into the front pocket formed by the hydrophobic side chains of the Schellman loop and α-D loop in a similar manner to the modeled structure

Table 1. Initial Front Pocket Studies
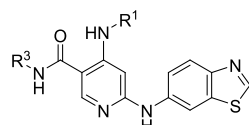
Cmpd	R[1]	R[3]	IRAK4[a] IC$_{50}$ (nM)	PBMC[b] IC$_{50}$ (nM)	hWB[b] IC$_{50}$ (nM)	LM Stability[c] (H, Ms % rem)	Fold sel LCK[d]
5	i-pr		15	NT[e]	NT	74, 45	NT
6	i-pr		12	NT	NT	52, 32	NT
7	i-pr		7	NT	NT	55, 31	NT
8	i-pr	HO	24	6,900	NT	84, 87	16
9	i-pr	HO	4.1±0.3 (n=3)	290	1,100	79, 68	104
10	cyc-pr	HO	10	290	900	65, 99	200
11	i-pr	HO ... F	2.4±1.1 (n=6)	480±100 (n=4)	2,000±1500 (n=3)	92, 86	270
12	cyc-pr	HO ... F	2.4±0.8 (n=3)	230±110 (n=7)	810	90, 89	170
13	i-pr	HO ... F	19	2,900	NT	NT	NT
14	i-pr	HO ... F F	4.3	570±290 (n=4)	2,800	71, 61	320
15	cyc-pr	HO ... F	9.3	730	NT	NT	110

[a]Kinase activity was measured by Caliper assay. [b]LTA-induced IL6 assay. Values represent mean IC$_{50}$ ± SD. All compounds were tested in duplicate unless otherwise noted. [c]Liver microsomal stability assays were typically single determinations. [d]LCK IC$_{50}$/IRAK4 IC$_{50}$. [e]NT, not tested.
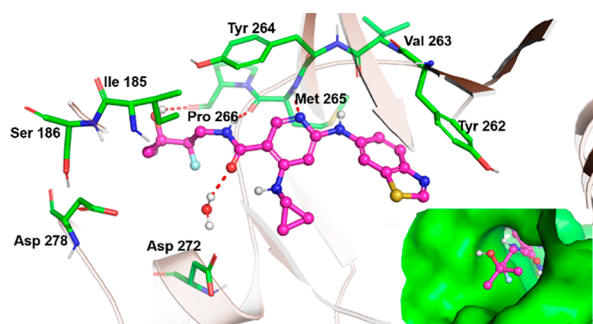

Figure 3. Co-crystal structure of **12** with IRAK4 (PDB code 6VQL).

of **4** in IRAK4. The dimethyl groups point toward the hydrophobic residues Ile185 and Val187, and those increased lipophilic interactions may explain the increase in binding from **8** to **9**. The increase in cLogD (pH 7.4) from **8** to **9** is consistent with this observation (1.70 vs 2.44, respectively).[18] The cyclopropyl group at C4 makes a hydrophobic contact with Val200 of the glycine rich p-loop (interaction not shown); the benzothiazole ring at C2 is engaged in a π-stacking interaction with gatekeeper residue Tyr262, and the pyridine N and amide NH engage the hinge by interacting with Met265 and Pro266, respectively.

Further profiling data revealed that **12** was more potent in mouse whole blood (mWB IC$_{50}$ 240 nM) than human whole blood (hWB IC$_{50}$ 810 nM). In a mouse PK study at 10 mg/kg, po, serum concentrations greater than the mouse whole blood IC$_{50}$ were observed up to 3 h postdose (data not shown). This

level of target coverage in circulation provided an opportunity to test the ability of **12** to block IRAK4-mediated responses in vivo.

Compound **12** inhibited IL-6 production in an LTA-induced (TLR2 driven) acute model of murine inflammation with maximal suppression observed at doses ≥25 mg/kg (Figure 4).[9]
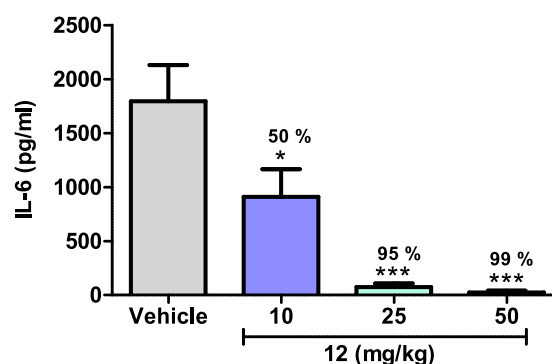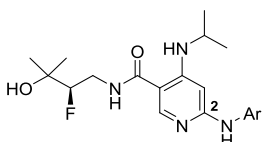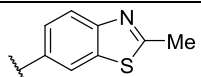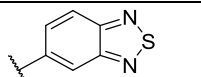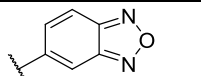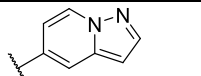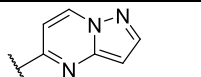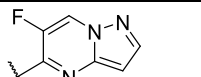

Figure 4. In vivo inhibition of a TLR2−IRAK4 mediated PD response in mice. Data are from one experiment with 8 animals per group: **$p < 0.01$, ***$p < 0.0001$; one-way ANOVA with a Dunnett test.

Serum concentrations for the 10, 25, and 50 mg/kg doses at time of IL-6 measurement were 410, 4500, and 9600 nM, respectively, consistent with robust levels of target coverage. Due to the relatively poor PK profile of **12** (Table 3), in addition to a weak human whole blood potency of 810 nM, it was considered a challenge to advance this molecule beyond murine studies. Subsequently, we turned our attention to optimizing the

Table 2. SAR on the Gatekeeper Interacting Fragment

Cmpd	Ar	IRAK4 IC$_{50}$ (nM)[a]	PBMC IC$_{50}$ (nM)[b]	hWB IC$_{50}$ (nM)[b]	Liver Micro-somal Stability (H, Ms %rem)[c]	LCK fold sel	cKit fold sel	SI33[c]
16	benzothiazole-2-Me	8	1,700	12,000	92, 78	3,500	6,200	3.5
17	benzothiadiazole	3.5±2.6 (n=5)	320±130 (n=4)	1,160	74, 80	93	>15,000	1.0
18	benzooxadiazole	8.7±2.5 (n=5)	640±280 (n=4)	210±60 (n=3)	93, 89	190	420	1.5
19	pyrazolopyridine	5.2±1.1 (n=5)	410±220 (n=3)	650±900 (n=4)	78, 85	>380	240	3.9
20	pyrazolopyrimidine	3.2±0.6 (n=4)	100	340±220 (n=7)	100, 89	130	8	7.8
21	F-pyrazolopyrimidine	3.4±1.1 (n=6)	370±300 (n=4)	920±490 (n=8)	93, 89	>590	>590	1

[a]Kinase activity was measured by Caliper assay. [b]LTA-IL6 assay. All compounds were tested in duplicate unless otherwise noted. [c]Liver microsomal stability and kinome selectivity assays were typically single determinations. Kinome selectivity screens were done at a single concentration of 1 μM.

C2 heterocycle in an attempt to identify compounds with improved bioavailability and reduced clearance to enable to longer-term efficacy studies.

Having evaluated the C4 and amide substituent previously, a campaign was undertaken to identify an improved π-stacking heterocycle at the C2 position. Maintaining whole blood potency and kinome selectivity while improving PK parameters to enable longer-term efficacy studies was the focus of this effort. The results are summarized in Table 2. Metabolite profiling of **12** revealed a degree of oxidation at the benzothiazole C2 position. Accordingly, a methyl group was incorporated at the benzothiazole in an attempt to block that metabolism; however, analog **16** suffered from reduced human whole blood potency. Benzothiadiazole and benzooxadiazole analogs **17** and **18** were potent against IRAK4 with **18** showing promise in hWB and kinase selectivity (SI$_{33}$ of 1.5). In vitro biotransformation data (not shown) demonstrated that the 1,2,5-oxadiazole ring of **18** was susceptible to ring opening and glutathione conjugation. Efforts then focused on the all nitrogen heterocycles **19–21**. Pyrazolopyridine **19** and pyrazolopyrimidine **20** demonstrated a good balance of enzyme, cellular, and hWB potencies and excellent liver microsomal stability. However, **20** demonstrated an erosion of kinome wide selectivity (SI$_{33}$ 7.8). We determined IC$_{50}$ values on ∼70 kinases, and 11 kinases were inhibited with an IC$_{50}$ of less than 1 μM (TNIK 8 nM; cKIT 24 nM;[19] TAK1 190 nM; see SI for additional IC$_{50}$ data).

Since inhibiting cKIT and TAK1 has the potential to confer toxicity and impart confounding immune suppression activity

(via the TAK/NFκB pathway), we modeled compound **20** in a published cKIT crystal structure (PDB 4HVS), Figure 5 inset.
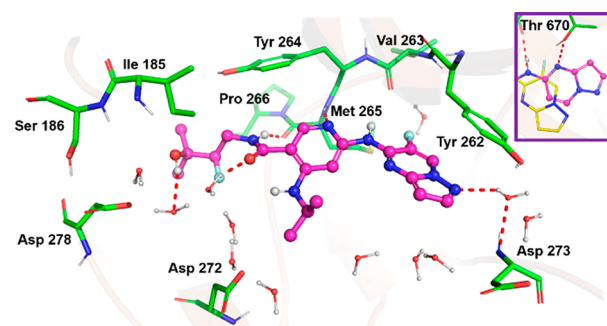

Figure 5. Co-crystal structure of **21** with IRAK4. Apart from the other interactions displayed by **12**, a water-mediated interaction with Asp329 was also seen (PDB 6LXY). Inset, model of **20** and **21** with the cKIT gatekeeper region.

Modeling suggests that the pyridine makes similar hinge region interactions in both cKIT and IRAK4; however, there is a difference in the way the pyrazolopyrimidine moiety may interact with these kinases. In the case of IRAK4, the pyrazolopyrimidine heterocycle π-stacks with the gatekeeper Tyr262, whereas the conformation of the heterocycle may flip and engage with the side chains of Thr670 (gatekeeper) and Asp810 of cKIT. Arguably, these H-bonds confer cKIT potency for this compound. The fact that the compound is inactive on

Table 3. Mouse PK Data of Select Molecules

compd	Caco-2 (nm/s)	dose, mg/kg (iv/po)	CL (mL·min^{-1}·kg^{-1})	V_{ss} (L/kg)	$T_{1/2}$ (h)	AUC (μM·h) (iv/po)	F%
12	81	2/10	47	2.1	2.2	1.6/3.3	40
18	38	2/3	14	3.2	3.6	4.7/4.6	65
20	69	2/2	33	3	2	2.4/0.9	36
21	215	2/5	15	2	1.4	5/24	>100

the Thr670Ile mutant of cKIT lent further credence to this hypothesis.[20] We then reasoned that it was possible to disturb the binding conformation of this heterocycle on cKIT by substitution on the 6-position of the pyrazolopyrimidine, resulting in **21**. The improvement in kinome selectivity of **21** (SI$_{33}$ 1.0) based on a single F substitution was remarkable. We determined discrete IC$_{50}$ values on 119 kinases for **21**, and only three kinases were inhibited with an IC$_{50}$ of less than 1 μM (TNIK 130 nM; IRAK3 760 nM, TYRO3 980 nM). cKIT and LCK IC$_{50}$ values were >2000 nM. While we were unable to obtain a crystal structure of **21** bound to cKIT, modeling suggested that the gatekeeper interacting heterocycle switched back to a conformation similar to that of the compound on IRAK4 (Figure 5). This results in the loss of H-bonds with cKIT gatekeeper fragment Thr670 and Asp810 residues providing an improved selectivity profile for compound **21**.

Encouraged by the dramatic improvement in the kinase selectivity achieved by the introduction of a single fluorine, **21** was profiled in a series of in vitro assays. Compound **21** was potent in cells (PBMC, 370 nM) and moderately potent in human (920 nM) and mouse (370 nM) whole blood. It was determined that **21** possessed excellent Caco-2 permeability (A → B, 215 nm/s) and robust liver microsomal stability (>90% rem in HLM and MLM). Pharmacokinetic evaluation in mice (Table 3) revealed low clearance and high bioavailability relative to other key molecules in this effort. Compound **21** exhibited robust inhibition of IL-6 (murine PD, Figure 6) at all doses with
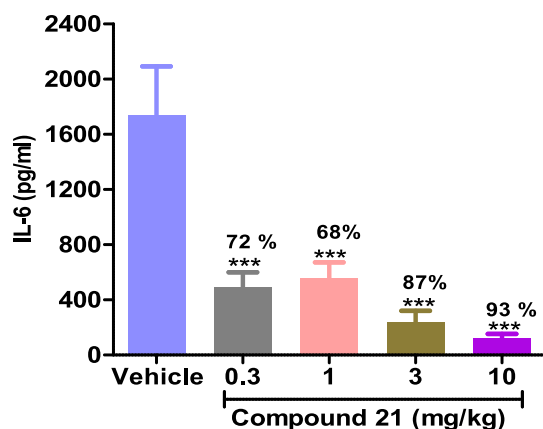
Figure 6. Efficacy of **21** in the LTA-induced IL-6 pharmacodynamic model: ***$p < 0.0001$, one-way ANOVA with a Dunnett test.

the highest dose (10 mg/kg) exhibiting almost complete inhibition of IL-6.[21] This represents a significant improvement in the dose response relationship compared to compound **12**. The good pharmacodynamic response, excellent oral bioavailability, and high kinome selectivity suggested that **21** would be a suitable compound to test in a murine model of IRAK4 driven inflammation. To that end, **21** was taken into a 6 day imiquimod-induced murine model of psoriasis and displayed a dose dependent improvement of the clinical signs of psoriasis

after 6 days of dosing (Figure 7).[22] In addition, the drug was well tolerated in these animals.
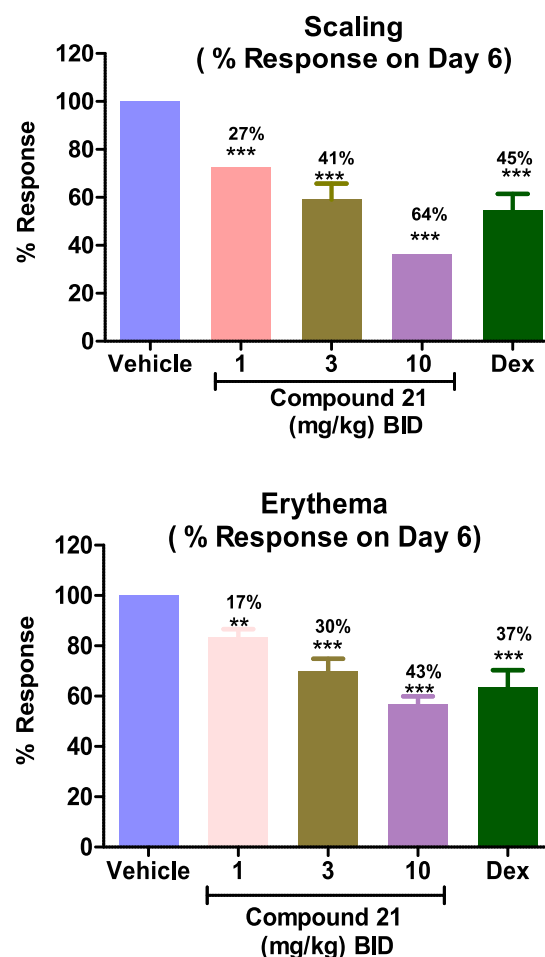
Figure 7. Efficacy of **21** in the imiquimod induced psoriasis model. Dex = dexamethasone; **$p < 0.001$, ***$p < 0.0001$, one-way ANOVA with a Dunnett test.

The synthesis of described analogs is depicted in Scheme 1. Ethyl 4,6-dichloro nicotinate (**22**) was converted into the corresponding 4-alkylamino derivative (**23**), which was then hydrolyzed to acid (**24**). Coupling of **24** with (*R*)-4-amino-3-fluoro-2-methylbutan-2-ol (**30**, Scheme 2) provided nicotinamide (**25**). Subsequent amination with aryl amines under Buchwald conditions afforded target compounds (**26**). (*R*)-4-Amino-3-fluoro-2-methylbutan-2-ol was synthesized from a chiral pool serine ethyl ester **27** following synthetic Scheme 2.[23] 6-Fluoropyrazolo[1,5-*a*]pyrimidin-5-amine was prepared according to the procedures outlined in Scheme 3. Briefly, 5-amino pyrazole was condensed with diethyl 2-fluoromalonate to afford **32**. Subsequent bis-chlorination to **33** and selective amination afforded **34**. Reductive deamination afforded **35** in

**Scheme 1. Synthesis of Nicotinamide Based IRAK4 Inhibitors**[a]
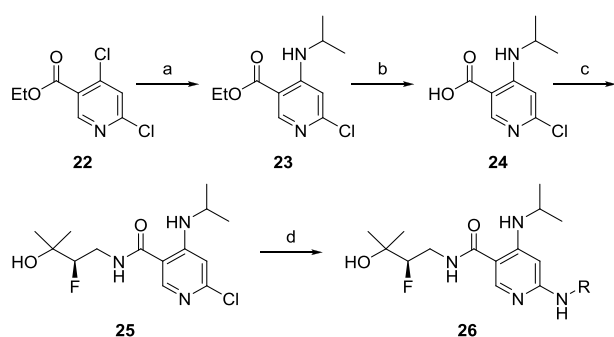
[a]Conditions: (a) isopropyl amine, DIPEA, DMA, 90 °C, 6 h, 84%; (b) LiOH, EtOH/H$_2$O (2:1), 25 °C, 2h, 99%; (c) **30**, HATU, DIPEA, DMF, 0 to 25 °C, 64%; (d) R-NH$_2$, Pd$_2$(dba)$_3$, XantPhos, Na$_2$CO$_3$, dioxane, 110 °C, 12−16 h, 5−40%.

Scheme 2. Synthesis of Fluoropropanol Fragment[a]
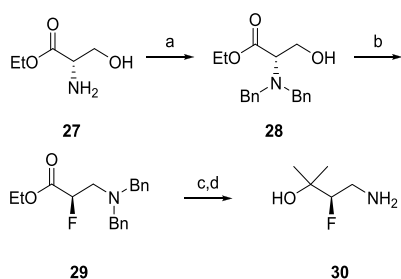
[a]Conditions: (a) benzyl bromide, K$_2$CO$_3$, KI, DMF, 16 h, 92%; (b) DAST, DCM, −40 to 25 °C, 1 h, 87%; (c) CH$_3$MgBr, THF, 0 °C to rt, 82%; (d) Pd/C, Pd(OH)$_2$, H$_2$, MeOH, 6 h, 97%.

Scheme 3. Synthesis of 6-Fluoropyrazolo[1,5-*a*]pyrimidin-5-amine Fragment[a]
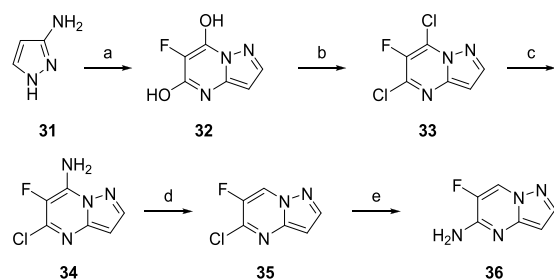
[a]Conditions: (a) Na, EtOH, diethyl 2-fluoromalonate, reflux, 4 h, 73%; (b) POCl$_3$, reflux, 16 h, 65%; (c) aq. NH$_4$OH, 80 °C, 12 h, 97%; (d) isoamyl nitrite, dioxane, reflux, 2 h, 93%; (e) NH$_4$OH, 75 °C, 3 h, 94%.

high yield, which was converted to the desired fragment **36** upon reaction with NH$_4$OH.

In summary, we disclose the discovery of a highly selective and potent IRAK4 inhibitor guided by structural information. By extending the amide side chain to occupy the front pocket, we improved potency as well as selectivity against off-target kinases. Exploration of a limited number of π-stacking fragments led to the identification of compounds with improved pharmacokinetic parameters. Finally, we were able to improve kinase selectivity by the rational incorporation of a single fluorine atom to yield compound **21**. Nicotinamide **21** provided a robust PD effect in an LTA-induced model of acute inflammation with

>90% inhibition at a 10 mg/kg dose. Efficacy in a short-term model of murine psoriasis was demonstrated with robust inhibition of disease end points in a dose dependent fashion. The progression of this chemical series to advanced preclinical and clinical assets will be the subject of future communications.

■ ASSOCIATED CONTENT

ⓢ Supporting Information

The Supporting Information is available free of charge at https://pubs.acs.org/doi/10.1021/acsmedchemlett.0c00082.

Full experimental details for key compounds, biological protocols, screening protocols, kinome selectivity tables, and modeling methods (PDF)

■ AUTHOR INFORMATION

Corresponding Authors

John Hynes, Jr. − *Research & Development, Bristol Myers Squibb, Princeton, New Jersey 08543, United States;* ⓞ orcid.org/0000-0002-0490-5179; Email: john.hynes@bms.com

Satheesh Nair − *Biocon Bristol Myers Squibb Research Center, Bangalore 560099, India;* Email: satheesh.nair@syngeneintl.com

Authors

Sreekantha Ratna Kumar − *Biocon Bristol Myers Squibb Research Center, Bangalore 560099, India*

Venkatram Reddy Paidi − *Biocon Bristol Myers Squibb Research Center, Bangalore 560099, India*

Ramesh Sistla − *Biocon Bristol Myers Squibb Research Center, Bangalore 560099, India*

Durgarao Kantheti − *Biocon Bristol Myers Squibb Research Center, Bangalore 560099, India*

Subba Rao Polimera − *Biocon Bristol Myers Squibb Research Center, Bangalore 560099, India*

Soodamani Thangavel − *Biocon Bristol Myers Squibb Research Center, Bangalore 560099, India*

Amrita Jha Mukherjee − *Biocon Bristol Myers Squibb Research Center, Bangalore 560099, India*

Mitalee Das − *Biocon Bristol Myers Squibb Research Center, Bangalore 560099, India*

Rajeev S. Bhide − *Research & Development, Bristol Myers Squibb, Princeton, New Jersey 08543, United States*

William J. Pitts − *Research & Development, Bristol Myers Squibb, Princeton, New Jersey 08543, United States*

Natesan Murugesan − *Research & Development, Bristol Myers Squibb, Princeton, New Jersey 08543, United States*

Shailesh Dudhgoankar − *Biocon Bristol Myers Squibb Research Center, Bangalore 560099, India*

Jignesh Nagar − *Biocon Bristol Myers Squibb Research Center, Bangalore 560099, India*

Siva Subramani − *Biocon Bristol Myers Squibb Research Center, Bangalore 560099, India*

Debarati Mazumder − *Biocon Bristol Myers Squibb Research Center, Bangalore 560099, India*

Julie A. Carman − *Research & Development, Bristol Myers Squibb, Princeton, New Jersey 08543, United States*

Deborah A. Holloway − *Research & Development, Bristol Myers Squibb, Princeton, New Jersey 08543, United States*

Xin Li − *Research & Development, Bristol Myers Squibb, Princeton, New Jersey 08543, United States*

Mark P. Fereshteh − *Research & Development, Bristol Myers Squibb, Princeton, New Jersey 08543, United States*

Stefan Ruepp — *Research & Development, Bristol Myers Squibb, Princeton, New Jersey 08543, United States*

Kamalavenkatesh Palanisamy — *Biocon Bristol Myers Squibb Research Center, Bangalore 560099, India*

T. Thanga Mariappan — *Biocon Bristol Myers Squibb Research Center, Bangalore 560099, India*

Srinivas Maddi — *Biocon Bristol Myers Squibb Research Center, Bangalore 560099, India*

Ajay Saxena — *Research & Development, Bristol Myers Squibb, Princeton, New Jersey 08543, United States*

Paul Elzinga — *Research & Development, Bristol Myers Squibb, Princeton, New Jersey 08543, United States*

Anjaneya Chimalakonda — *Research & Development, Bristol Myers Squibb, Princeton, New Jersey 08543, United States*

Qian Ruan — *Research & Development, Bristol Myers Squibb, Princeton, New Jersey 08543, United States*

Kaushik Ghosh — *Biocon Bristol Myers Squibb Research Center, Bangalore 560099, India*

Sucharita Bose — *Biocon Bristol Myers Squibb Research Center, Bangalore 560099, India*

John Sack — *Research & Development, Bristol Myers Squibb, Princeton, New Jersey 08543, United States*

Chunhong Yan — *Research & Development, Bristol Myers Squibb, Princeton, New Jersey 08543, United States*

Susan E. Kiefer — *Research & Development, Bristol Myers Squibb, Princeton, New Jersey 08543, United States*

Dianlin Xie — *Research & Development, Bristol Myers Squibb, Princeton, New Jersey 08543, United States*

John A. Newitt — *Research & Development, Bristol Myers Squibb, Princeton, New Jersey 08543, United States*

S. Pon Saravanakumar — *Biocon Bristol Myers Squibb Research Center, Bangalore 560099, India*

Richard A. Rampulla — *Research & Development, Bristol Myers Squibb, Princeton, New Jersey 08543, United States*

Joel C. Barrish — *Research & Development, Bristol Myers Squibb, Princeton, New Jersey 08543, United States*

Percy H. Carter — *Research & Development, Bristol Myers Squibb, Princeton, New Jersey 08543, United States*

Complete contact information is available at:
https://pubs.acs.org/10.1021/acsmedchemlett.0c00082

Author Contributions

The manuscript was written through contributions of all authors.

Notes

The authors declare no competing financial interest.

ABBREVIATIONS

TLR, Toll-like receptors; IRAK, interleukin-receptor associated kinase; TNFα, tumor necrosis factor alpha; SLE, systemic lupus erythematosus; PBMC, peripheral blood mononuclear cells; LTA, lipoteichoic acid; LCK, lymphocyte-specific protein tyrosine kinase; hWB, human whole blood; HLM, human liver microsomes; MLM, mouse liver microsomes; TAK1, transforming growth factor beta-activated kinase 1; DIPEA, diisopropyl amine; DMA, dimethylacetamide; EtOH, ethanol; HATU, 1-[bis(dimethylamino)methylene]-1*H*-1,2,3-triazolo-[4,5-*b*]pyridinium 3-oxid hexafluorophosphate; DMF, dime-thylformamide; XantPhos, 4,5-bis(diphenylphosphino)-9,9-di-methylxanthene; DAST, diethylaminosulfur trifluoride; DCM, dichloromethane; THF, tetrahydrofuran; MeOH, methanol

REFERENCES

(1) Takeda, K.; Kaisho, T.; Akira, S. Toll-like receptors. *Annu. Rev. Immunol.* **2003**, *21*, 335−376.

(2) Akira, S.; Takeda, K. Toll-like receptor signaling. *Nat. Rev. Immunol.* **2004**, *4*, 499−511.

(3) Li, S.; Strelow, A.; Fontana, E. J.; Wesche, H. IRAK4: a novel member of the IRAK family with the properties of an IRAK-kinase. *Proc. Natl. Acad. Sci. U. S. A.* **2002**, *99*, 5567−5572.

(4) O'Neill, L. A. The interleukin receptor/toll-like receptor superfamily: 10 years of progress. *Immunol. Rev.* **2008**, *226*, 10−18.

(5) Koziczak-Holbro, M.; Littlewood-Evans, A.; Pöllinger, B.; Kovarik, J.; Dawson, J.; Zenke, G.; Burkhart, C.; Müller, M.; Gram, H. The critical role of kinase activity of interleukin-1 receptor-associated kinase 4 in animal models of joint inflammation. *Arthritis Rheum.* **2009**, *60*, 1661−1671.

(6) Suzuki, N.; Suzuki, S.; Duncan, G. S.; Millar, D. G.; Wada, T.; Mirtsos, C.; Takada, H.; Wakeham, A.; Itie, A.; Li, S.; Penninger, J. M.; Wesche, H.; Ohashi, P. S.; Mak, T. W.; Yeh, W.-C. Severe impairment of interleukin-1 and Toll-like receptor signalling in mice lacking IRAK-4. *Nature* **2002**, *416*, 750−754.

(7) Picard, C.; Puel, A.; Bonnet, M.; Ku, C.-L.; Bustamante, J.; Yang, K.; Soudais, C.; Dupuis, S.; Feinberg, J.; Fieschi, C.; Elbim, C.; Hitchcock, R.; Lammas, D.; Davies, G.; Al-Ghonaium, A.; Al-Rayes, H.; Al-Jumaah, S.; Al-Hajjar, S.; Al-Mohsen, I. Z.; Frayha, H.; Rucker, R.; Hawn, T. R.; Aderem, A.; Tufenkeji, H.; Haraguchi, S.; Day, N. K.; Good, R. A.; Gougerot-Pocidalo, M. A.; Ozinsky, A.; Casanova, J. L. Pyrogenic bacterial infections in humans with IRAK-4 deficiency. *Science* **2003**, *299*, 2076−2079.

(8) Ku, C.-L.; von Bernuth, H.; Picard, C.; Zhang, S.-Y.; Chang, H.-H.; Yang, K.; Chrabieh, M.; Issekutz, A. C.; Cunningham, C. K.; Gallin, J.; Holland, S. M.; Roifman, C.; Ehl, S.; Smart, J.; Tang, M.; Barrat, F. J.; Levy, O.; McDonald, D.; Day-Good, N. K.; Miller, R.; Takada, H.; Hara, T.; Al-Hajjar, S.; Al-Ghonaium, A.; Speert, D.; Sanlaville, D.; Li, X.; Geissmann, F.; Vivier, E.; Maródi, L.; Garty, B. Z.; Chapel, H.; Rodriguez-Gallego, C.; Bossuyt, X.; Abel, L.; Puel, A.; Casanova, J. L. Selective predisposition to bacterial infections in IRAK-4 deficient children: IRAK-4 dependent TLR's are otherwise redundant in protective immunity. *J. Exp. Med.* **2007**, *204*, 2407−2422.

(9) Dudhgaonkar, S.; Ranade, S.; Nagar, J.; Subramani, S.; Prasad, D. S.; Karunanithi, P.; Srivastava, R.; Venkatesh, K.; Selvam, S.; Krishnamurthy, P.; Mariappan, T. T.; Saxena, A.; Fan, L.; Stetsko, D. K.; Holloway, D. A.; Li, X.; Zhu, J.; Yang, W.; Ruepp, S.; Nair, S.; Santella, J.; Duncia, J.; Hynes, J.; McIntyre, K. W.; Carman, J. A. Selective IRAK4 inhibition attenuates disease in murine lupus models and demonstrates steroid sparing activity. *J. Immunol.* **2017**, *198*, 1308−1309.

(10) For a recent review of IRAK4 inhibitors, see McElroy, W. T. Interleukin-1 receptor-associated kinase 4 (IRAK4) inhibitors: and updated patent review (2016−2018). *Expert Opin. Ther. Pat.* **2019**, *29*, 243−259.

(11) Lee, K. L.; Ambler, C. M.; Anderson, D. R.; Boscoe, B. P.; Bree, A. G.; Brodfuehrer, J. I.; Chang, J. S.; Choi, C.; Chung, S.; Curran, K. J.; Day, J. E.; Dehnhardt, C. M.; Dower, K.; Drozda, S. E.; Frisbie, R. K.; Gavrin, L. K.; Goldberg, J. A.; Han, S.; Hegen, M.; Hepworth, D.; Hope, H. R.; Kamtekar, S.; Kilty, I. C.; Lee, A.; Lin, L.-L.; Lovering, F. E.; Lowe, M. D.; Mathias, J. P.; Morgan, H. M.; Murphy, E. A.; Papaioannou, N.; Patny, A.; Pierce, B. S.; Rao, V. R.; Saiah, E.; Samardjiev, I. J.; Samas, B. M.; Shen, M. W. H.; Shin, J. H.; Soutter, H. H.; Srohback, J. W.; Symanowicz, P. T.; Thomason, J. R.; Trzupek, J. D.; Vargas, R.; Vincent, F.; Yan, J.; Zapf, C. W.; Wright, S. W. Discovery of clinical candidate 1-{[(2S, 3S, 4S)-3-ethyl-4-fluoro-5-oxopyrroli-din—2-yl]methoxy}-7-methoxyisoquinoline-6-carboxamide (PF-06650833), a potent, selective inhibitor of interleukin-1 receptor

associated kinase 4 (IRAK4), by fragment-based drug design. *J. Med. Chem.* **2017**, *60*, 5521−5542.

(12) Danto, S.; Shojaee, N.; Singh, R. S. P.; Manukyan, Z.; Mancuso, J.; Peeva, E.; Vincent, M.; Beebe, J. Efficacy and Safety of the Selective Interleukin-1 Receptor Associated Kinase 4 Inhibitor, PF-06650833, in Patients with Active Rheumatoid Arthritis and Inadequate Response to Methotrexate. Presented at the 2019 ACR/ARP Annual Meeting, Atlanta, GA, November 8−11, 2019. Abstract 2909.

(13) Bhide, R. S.; Keon, A.; Weigelt, C.; Sack, J. S.; Schmidt, R. J.; Lin, S.; Xiao, H.-Y.; Spergel, S. H.; Kempson, J.; Pitts, W. J.; Carman, J.; Poss, M. A. Discovery and structure-based design of 4,6-diaminonicotinamides as potent and selective IRAK4 inhibitors. *Bioorg. Med. Chem. Lett.* **2017**, *27*, 4908−4913.

(14) SI_{33} is the ratio of number of kinases with <33% activity remaining compared to control divided by the number of kinases tested at 1 aM concentration. See Cheng, A. C.; Eksterowicz, J.; Geuns-Meyer, S.; Sun, Y. Analysis of kinase inhibitor selectivity using a thermodynamics-based partition index. *J. Med. Chem.* **2010**, *53*, 4502−4510.

(15) Davis, S. J.; van der Merwe, P. A. Lck and the nature of the T cell receptor trigger. *Trends Immunol.* **2011**, *32*, 1−5.

(16) Kuglstatter, A. I.; Villasenor, A. G.; Shaw, D.; Lee, S. W.; Tsing, S.; Niu, L.; Song, K. W.; Barnett, J. W.; Browner, M. Cutting Edge: IL-1 receptor-associated kinase 4 structures reveal novel features and multiple conformations. *J. Immunol.* **2007**, *178*, 2641−2645.

(17) Gillis, E. P.; Eastman, K. J.; Hill, M. D.; Donnelly, D. J.; Meanwell, N. A. Applications of Fluorine in Medicinal Chemistry. *J. Med. Chem.* **2015**, *58*, 8315.

(18) Clogd was calculated using the logD plugin in *Instant JChem*. (version 18.22.5) from Chemaxon (www.chemaxon.com, Chemaxon, Cambridge, MA).

(19) In a cKIT-dependent functional assay, **20** demonstrated an IC_{50} of 170 nM.

(20) In a double mutant of cKIT (Val559Asp and Thr670Ile), **20** did not bind in the Ambit panel. The Val559Asp single mutant had significant binding in the Ambit panel indicating that the loss of binding of **20** was due solely to the Thr670 change in the double mutant. See Supporting Information for the kinome panel results.

(21) Exposures of **21** at the 2 h time point were 42, 400, 1950, and 9400 nM at 0.3, 1, 3, and 10 mg/kg doses, respectively.

(22) Exposures of **21** at 8 h time point were 12, 31, and 494 nM at 1, 3, and 10 mg/kg doses, respectively.

(23) Ishii, A.; Yamazaki, T.; Yasumoto, M.; Masuda, T.; Tsuruta, H. U.S. Patent 8217196, 2012.